Eur Biophys J (1998) 28: 26–37

ARTICLE

Joachim Wegener · Andreas Janshoff
Hans-Joachim Galla

Cell adhesion monitoring using a quartz crystal microbalance: comparative analysis of different mammalian cell lines

Received: 26 January 1998 / Revised version: 21 April 1998 / Accepted: 4 May 1998

Abstract The quartz crystal microbalance (QCM) has been widely accepted as a sensitive technique to follow adsorption processes in gas as well as in liquid environments. However, there are only a few reports about the use of this technique to monitor the attachment and spreading of mammalian cells onto a solid support in culture. Using a QCM-setup we investigated the time course of cell attachment and spreading as a function of seeding density for three widespread and frequently used cell lines (MDCK strains I and II and Swiss 3T3-fibroblasts). Results were found to be in good agreement with the geometrical properties of the individual cell types. The shifts of the resonance frequency associated with confluent cell layers on top of the quartz resonators were found to be dependent on the cell species [MDCK-I: (320±20) Hz; MDCK-II: (530±25) Hz; 3T3: (240±15) Hz] reflecting their individual influence on the shear oscillation of the resonator. These findings are discussed with respect to the basic models of materials in contact with an oscillating quartz resonator. We furthermore showed by inhibition-assays using soluble RGD-related peptides, that only specific, integrin mediated cell adhesion is detected using this QCM approach, whereas the sole presence of the cellular body in close vicinity to the resonator surface is barely detectable.

Key words Quartz crystal microbalance · Cell adhesion · Cell-substrate interaction · RGD-sequence

Abbreviations *QCM* Quartz crystal microbalance · *PBS* Phosphate buffered saline without divalent cations · *PBS*$^{++}$ Phosphate buffered saline with 0.5 mM Mg^{2+} and 1 mM Ca^{2+}; *ZO-1*: tight junction (*zonula occludens*) associated protein ZO-1 · *ECM* Extracellular matrix · *MDCK* Madin-Darby Canine-Kidney cells · *EDTA* Ethylenediaminetetraacetate · *BSA* Bovine serum albumin · *RGD* Arg-Gly-Asp · *GRGDS* Gly-Arg-Gly-Asp-Ser · *SDGRG* Ser-Asp-Gly-Arg-Gly

J. Wegener · A. Janshoff · H.-J. Galla (✉)
Institut für Biochemie,
Westfälische Wilhelms-Universität Münster,
Wilhelm-Klemm-Strasse 2,
D-48149 Münster, Germany
e-mail: GallaH@uni-muenster.de

Introduction

The attachment and spreading of mammalian cells on a surface in vitro is a rather complex and versatile process that depends on a variety of cellular and extracellular molecules and can be strongly affected by the particular culture conditions. Much work has been done to elucidate in detail the adhesion behavior of different cell species on tissue culture surfaces (Taylor 1961; Cornell 1969; Gallez 1994), which have often been modified by coating with proteins derived from the extracellular matrix, such as collagen, laminin or fibronectin (Aplin et al. 1984). These studies provide important information about the different molecular mechanisms responsible for cell attachment and spreading, thus giving valuable insight into the interactions of cells with the extracellular matrix (ECM) components that are important for various physiological processes such as cell differentiation during development, tissue regeneration or cell migration in tumor metastasis (Poste and Fidler 1980). Cell-substrate interactions are also of interest from a more technical point of view regarding the compatibility of biomaterial surfaces with living cells (Vogler 1988 and references therein).

The methods available for cell adhesion studies are very often based on cell counting, either of those cells attached to a particular surface (Ruoslahti et al. 1982) or of those remaining in the supernatant. Besides direct cell counting techniques, several indirect modifications have been described that are – for example – directed towards the quantification of total cell protein by colorimetric assays. Studies dealing with the morphological features of cell attachment and spreading on a solid substrate often employ time lapse videomicroscopy or ultrastructural techniques. These methods are, however, rather time consuming and labour intensive. In the case of microscopic evaluation of morpho-

logical aspects of cell attachment, interpretation of results is sometimes subjective in nature. Therefore, techniques that allow one to monitor the attachment and spreading of animal cells on a particular surface quantitatively and in real-time are highly desirable for all the purposes mentioned above. Mitra et al. (1991) recently introduced a very powerful technique based on electrical impedance measurements (electrical cell-substrate impedance sensing; ECIS) capable of monitoring the attachment and spreading of fibroblasts on planar gold electrodes ($< 0.1\ mm^2$) in real-time. This very elegant approach enables one to quantify coverage of the electrode surface in situ without disturbance of the adhesion process. The method was substantiated by comparing results with those of conventional assays.

Another promising approach to follow the adhesion and spreading of cells on solid substrates makes use of the quartz crystal microbalance (QCM) technique (Buttry and Ward 1992; Deakin and Buttry 1989), which – since Sauerbrey – is a well known tool to study deposition processes in the gas phase (Sauerbrey 1959). This QCM-technique comprises a thin (AT-cut)-quartz crystal sandwiched between two metal electrodes. Owing to its piezoelectric nature and crystal orientation shear vibrations of the quartz crystal lead to potential changes at these metal electrodes so that appropriate oscillator circuits can overcome energy losses and stabilize the shear vibration of the crystal at its resonance frequency. This resonance frequency alters when a foreign mass attaches to the piezoelectrically active surface. Within certain limits the observed frequency shift allows one to calculate the mass of the adsorbed material. Recent progress in designing oscillator circuits capable of coping with high viscous damping of the shear displacement allows one to apply this technique to monitor adsorption processes even in solution (Xu and Schlenoff 1995). However, as the quartz crystal is now in contact with a liquid phase, its resonance frequency is also affected by changes in the density or viscosity at the quartz-liquid interface as well as in the bulk phase (Kanazawa and Gordon 1985).

Despite the reasonable potential for applications in cell biology there are only very few reports in the literature dealing with adhesion monitoring of mammalian cells using a QCM (Redepenning et al. 1993; Gryte et al. 1993; Matsuda et al. 1992; Muratsugu et al. 1997). Redepenning and coworkers (1993) showed that the attachment and spreading of osteoblasts to such an oscillating quartz crystal can be monitored by recording the shift of the resonance frequency upon cell adhesion. The equilibrium frequency shift was reported to be linearly dependent on the fractional surface coverage as determined by scanning electron microscopic inspection of gradually covered resonators. Gryte et al. (1993) detected the attachment of African green monkey kidney (Vero) cells using this technique. These authors also followed the detachment of the cells upon lethal doses of NaOH. Matsuda et al. (1992) and Muratsugu et al. (1997) followed the adhesion of platelets to a QCM surface. However, only little is known about the mechanisms that are responsible for the frequency shift and its detailed interpretation. In a more recent study (Janshoff et al. 1996) we could experimentally prove by impedance analysis that cells, attached to an oscillating resonator, can not be treated like an adsorbed rigid mass and not as an entirely viscous material. However, a theoretical model to describe the rather complex behavior of attached cells is still lacking.

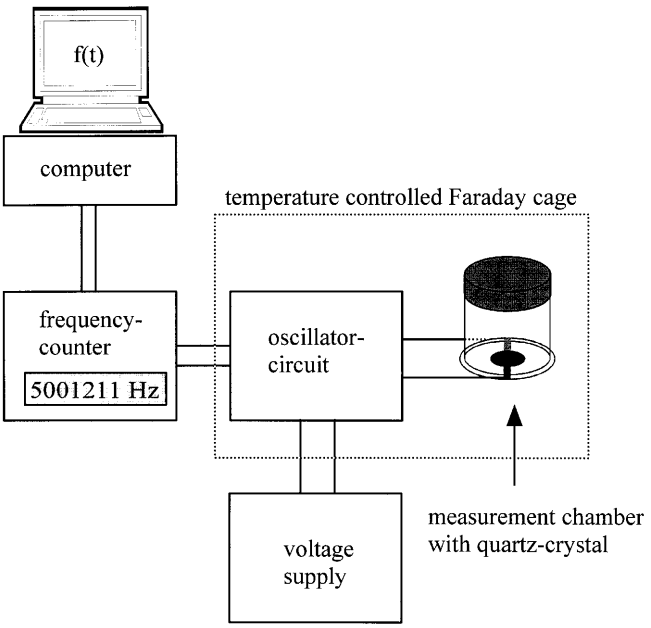

Fig. 1 Schematic diagram of the experimental setup used for QCM-measurements

In the present study we analyze the cell adhesion behavior of three different, very popular and widespread cell lines (MDCK strains I and II, Swiss 3T3-fibroblasts) as a function of the number of seeded cells by using a quartz crystal microbalance setup. For the first time different cell types are investigated using one and the same experimental apparatus, so that differences may be compared and attributed to cellular properties. We furthermore demonstrate that only specific, integrin-mediated cell adhesion to the quartz surface leads to the observed frequency changes, whereas the sole presence of the cellular body in close vicinity to the quartz surface is barely detectable. The QCM technique proved to be a very versatile and promising tool to study cell adhesion phenomena under a variety of external conditions.

Materials and methods

Apparatus

The experimental setup for QCM-measurements is schematically depicted in Fig. 1. The core component of the system is the quartz resonator, a plano-plano AT-cut quartz crystal (∅= 14 mm) with a fundamental resonance frequency of 5 MHz coated with gold electrodes (∅= 6 mm) on both sides (KVG, Niederbischofsheim, Germany). The electrodes were designed as shown in Fig. 1 with an area

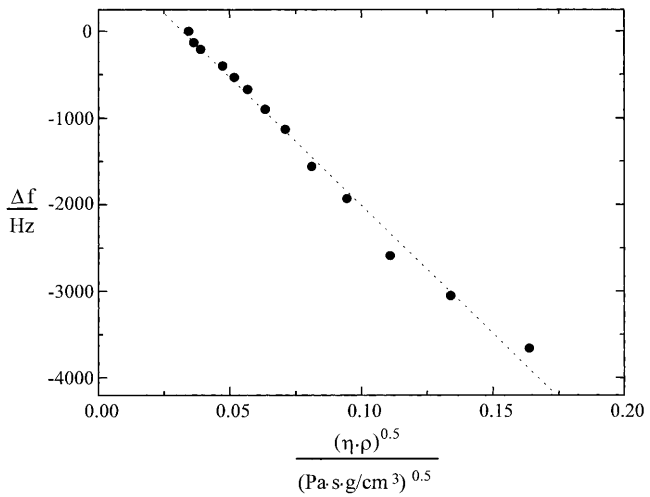

Fig. 2 Calibration of the QCM-setup with glycerol/water mixtures of different composition. The diagram depicts the final shifts of the resonance frequency (Δf) versus the square-root of the density-viscosity product for the particular solutions. The corresponding densities and viscosities were taken from the literature (Weast 1984). The resonance frequency of the quartz crystal in contact with a mixture of 5% glycerol and 95% water was arbitrarily set to zero. The *dotted line* represents the linear regression according to the Gordon-Kanazawa equation (2). The slope of the regression line is $(29.5\pm0.9) \cdot 10^3$ $(\mathrm{Pa} \cdot \mathrm{s} \cdot \mathrm{g/cm^3})^{1/2}$

of 0.33 cm^2. The measuring chamber was formed by fixing small glass tubes (cut-off upper parts of small glass vials) onto the quartz resonators with a silicon glue (Rhône Poulenc, Leverkusen, Germany). The gold electrodes were connected to the oscillator circuit via thin silver wires which were fixed to the gold electrodes of the quartz by a conductive adhesive (Epoxy-GmbH, Fürth/Odenwald, Germany). According to a recent paper of Teuscher and Garell (1995) this particular technique improves the stability of the oscillation significantly. Prior to any QCM-experiment the whole quartz dish was treated with an Argon plasma for three to five minutes in order to clean the electrode surface and to sterilize the chamber. The quartz dish was then mounted into a crystal holder, which fixes only the glued glass tube to avoid any contact with the quartz-crystal. Afterwards the measuring chamber was filled with the cell suspension, as detailed below, and subsequently closed by a screw cap in order to avoid evaporation of the liquid and gas exchange with ambient air. The quartz plate as well as the oscillator circuit were placed in a temperature controlled chamber which also serves as a Faraday cage. The temperature was kept at 37 °C. The oscillator circuit consists mainly of an integrated circuit SN74LS124N from Texas Instruments connected to a frequency counter from Hewlett Packard (HP 53181A). Data were collected using a common personal computer.

Calibration of the QCM

The integral mass sensitivity of the QCM was determined by electrodeposition of copper as described elsewhere (Hillier and Ward 1992). Deposition and frequency detection were performed under liquid loading. Following the theory of Sauerbrey (1959) the observed decrease in frequency should be proportional to the change in mass on the quartz resonator.

$$\Delta f = \frac{-2\ f_0^2\ \Delta m}{A\sqrt{\rho_q\ \mu_q}} = -\ C_f\ \Delta m \qquad (1)$$

where f_0 denotes the fundamental resonance frequency, A the electrode area, ρ_q the density of quartz ($\rho_q = 2.648$ g/cm^3) and μ_q the shear modulus of quartz ($\mu_q = 2.957 \cdot 10^{10}$ N/m^2). Those quantities combine to the integral mass sensitivity C_f which amounts to $0.032\ \mathrm{Hz} \cdot \mathrm{cm^2/ng}$ in our case. Though C_f is considerably lower than expected from Sauerbrey's equation (Eq. (1)) ($0.057\ \mathrm{Hz} \cdot \mathrm{cm^2/ng}$) the value is still reasonable considering the scrutiny of Hillier and Ward (1992) who predicted a similar value for 5 MHz plano-plano AT-cut quartz resonators plated with copper. They pointed out that plano-plano crystals suffer more energy loss from field fringing at the electrode edges than plano-convex quartz resonators.

Since the deposition of rigid copper-films is not well suited to model the adhesion of cells onto the quartz surface, we applied different well defined mixtures of glycerol/water to the resonator in order to calibrate the system to viscous loading as described elsewhere (Janshoff et al. 1996). Figure 2 depicts the change of resonance frequency as a function of the square root of the density-viscosity-product, which was calculated for the different solutions from literature data (Weast 1984). The change in resonance frequency for a 5% glycerol/95% water mixture is arbitrarily set to zero. The dotted line in Fig. 2 represents the linear regression according to the Gordon-Kanazawa (Kanazawa and Gordon 1985) equation (2) that predicts the shift in resonance frequency upon immersing a dry quartz crystal in solutions of different density (ρ_1) and viscosity (η_1) by the following relationship:

$$\Delta f = -\ f_0^{3/2} (\pi\ \rho_q\ \mu_q)^{-1/2}\ \sqrt{\eta_1\ \rho_1} = -\ A\ \sqrt{\eta_1\ \rho_1} \qquad (2)$$

The slope A of the regression line in Fig. 2 amounts to $(29.5 \pm 0.9) \cdot 10^3$ $(\mathrm{Pa} \cdot \mathrm{s} \cdot \mathrm{g/cm^3})^{1/2}$ compared to a theoretical value of $22.6 \cdot 10^3$ $(\mathrm{Pa} \cdot \mathrm{s} \cdot \mathrm{g/cm^3})^{1/2}$ as calculated from the values for f_0, ρ_q and μ_q.

Cell culture

Two strains of the epithelial cell-line MDCK (Madin-Darby Canine-Kidney), abbreviated MDCK-I and MDCK-II, as well as the murine fibroblastic cell-line 3T3 (Swiss) were investigated with respect to their cell adhesion behavior. Besides their individual morphology the two strains of MDCK cells I and II differ with respect to their ability to act as a selective barrier between two fluid compartments – probably the most important physiological function of any epithelial tissue. Whereas MDCK-I cells are classified as a tight epithelium with high transepithelial

electrical resistances (measure for barrier function with respect to ion permeabilities), MDCK-II cells belong to the so called leaky epithelia with moderate transepithelial resistances (Wegener et al. 1996). Both strains of MDCK cells were cultured identically. We used MEM-Earle (Biochrom, Berlin, Germany) as culture medium additionally supplemented with 4 mM glutamine (Biochrom), 100 mg/l penicillin (Biochrom), 100 mg/l streptomycin (Biochrom) and 10% (v/v) fetal calf serum (Gibco, Eggenstein, Germany). Stock flasks (10 cm^2) of these cell lines were grown in a humidified 5% CO_2/95% air atmosphere at 37 °C. Swiss-3T3 cells were grown in DMEM (Biochrom) culture medium using the same supplements as mentioned above. Stock flasks (10 cm^2) were maintained in an incubator with 10% CO_2/90% air atmosphere at 37 °C.

Cell adhesion monitoring

To aquire the time course of the resonance frequency during cell adhesion, the cells under investigation were removed from the stock flask by washing twice with phosphate buffered saline (PBS, without divalent cations) and subsequent trypsin digestion [0.25% (w/v) supplemented with 1 mM EDTA] for 20 minutes at 37 °C. Digestive cell removal was stopped by adding an excess of the particular culture medium. Cells were spun down by a 290×g centrifugation for 10 minutes. The pellet was resuspended in culture medium and aliquots of the cell suspension were transferred into the quartz dish. The remaining volume inside the dish was filled up by culture medium and the dish was then closed by a screw cap. Afterwards the whole dish was immediately mounted into the crystal holder and placed into the temperature controlled Faraday cage. The resonance frequency was recorded every 15 seconds. The number of cells seeded into the quartz dish was determined using an ordinary haemacytometer (Bürker). In those experiments in which cell adhesion was studied in the presence of peptides related to one of the integrin recognition sequences on extracellular matrix proteins (RGD), a corresponding amount of the particular stock solution of the peptide (in phosphate buffered saline; all purchased from Sigma, Deisenhofen, Germany) was added to the cell suspension within the quartz dish.

To discuss the time course of the resonance frequency shift in more detail, we estimated the cellular sedimentation behavior. Necessary quantities in this respect are cellular densities and their hydrodynamic radii. Cellular densities were determined as described elsewhere (Janshoff et al. 1996). Hydrodynamic radii of either cell species were determined from phase contrast micrographs of suspended cells and subsequent image processing.

Immunostaining of the tight junction associated protein ZO-1

Results of QCM-measurements will be discussed with respect to the surface areas of single cells within a confluent monolayer of either cell type. In the case of the fibroblastic 3T3-cells cellular surface areas were determined from phase contrast micrographs of confluent cell monolayers (see insert of Fig. 6b), using the intercellular cleft between adjacent cells as cell boundaries. In the case of epithelial and endothelial cells this can be performed more easily and accurately using fluorescence micrographs of immunostainings directed towards the tight junction associated protein ZO-1, which is exclusively localized at the cell perimeter of adjacent cells as shown in the fluorescent micrographs in the inserts of Figs. 3b and 5b. For this purpose MDCK-cells were washed twice with PBS^{++}, fixed with 4% paraformaldehyde for 15 min and subsequently permeabilized using 0.2% Triton-X 100 (v/v) for 5 min. Nonspecific binding sites were saturated by incubating for 15 min with a 3% BSA-solution (w/v) at room temperature. Monoclonal anti-ZO-1 antibodies derived from rat (Chemicon, Hermann Biermann GmbH, Bad Nauheim, Germany) were applied in a final concentration of 10 µg/ml for 90 minutes at 37 °C. Fluorescence-labeled anti-rat IgGs used as secondary antibodies were subsequently applied for 40 minutes at 37 °C in a final concentration of 10 µg/ml. The samples were inspected using a confocal laser scanning microscope (MRC-600, Biorad, München, Germany).

Results

Cell adhesion monitoring for different seeding densities

In the first part of the present study we investigated the adhesion of the three different cell species (MDCK-I, MDCK-II, Swiss 3T3) to the quartz surface dependent on the number of cells, seeded into the quartz dish at the beginning of the experiment.

MDCK-II

Figure 3a shows the change in resonance frequency of a quartz resonator in five individual experiments in which increasing amounts of MDCK-II cells were seeded onto the resonator at time zero. After an initial increase of the resonance frequency which is due to thermal equilibration of the resonator and the cell suspension from ambient temperature to the temperature of the incubation chamber (37 °C), the resonance frequency decreases during the next 3 h and reaches a new steady state value at the end of the observation time. In a control experiment (○) in which only culture medium but no cells were added to the quartz dish, the resonance frequency increases at the beginning of the experiment – as described above – but only a slight decrease (Δf_{max} = 18 Hz; here and throughout the entire study Δf_{max} denotes the modulus of the frequency shift) can be observed afterwards. As is obvious from Fig. 3a the maximum shift of the resonance frequency is dependent on the number of cells that were seeded onto the quartz surface and ranges between 150 Hz for $1.3 \cdot 10^5$ cells $\cdot$ cm^{-2} to

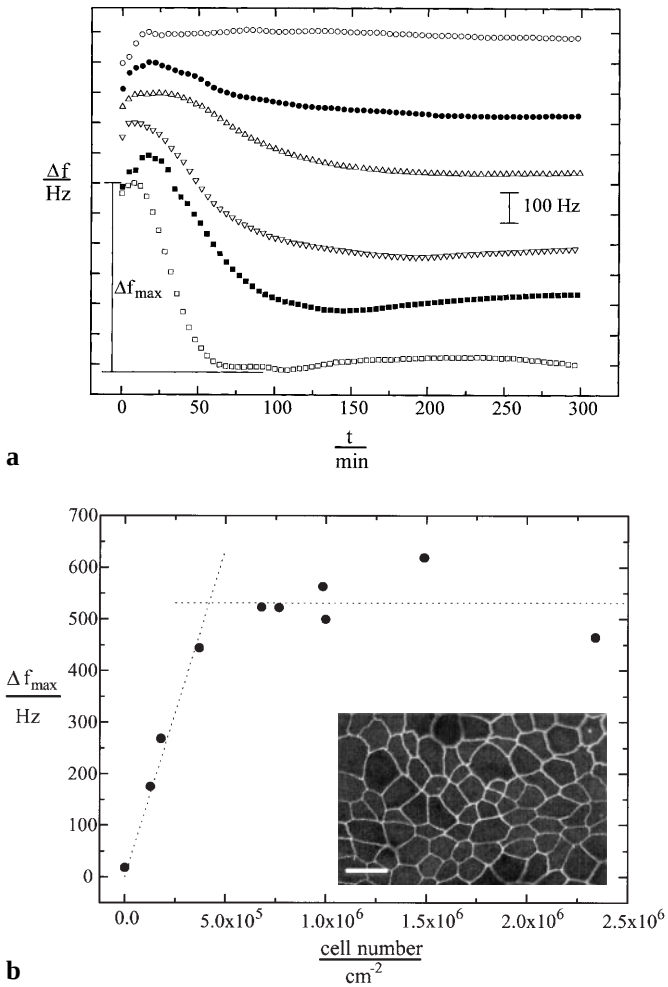

Fig. 3 **a** Time courses of the resonance frequency upon adhesion of increasing numbers of MDCK-II cells seeded into the quartz dish at time zero. The curve at the very top of the diagram (○) depicts the time course of the resonance frequency without addition of cells. The corresponding seeding densities in cells per cm^2: $1.3 \cdot 10^5$ (●); $1.8 \cdot 10^5$ (△); $3.7 \cdot 10^5$ (▽); $7.7 \cdot 10^5$ (■); $1.5 \cdot 10^6$ (□). Not all time courses considered in the following diagram **b** are depicted for the sake of clarity. **b** Maximum frequency shift as deduced from the time courses shown in part **a** as a function of seeding density for MDCK-II cells. The *dotted lines* represent regression lines according to our two case approach as detailed in the text. The slope of the ascending line amounts to $(1.2 \pm 0.1) \cdot 10^{-3}$ Hz/cells $\cdot$ cm^{-2}. The *horizontal line* depicts the frequency shifts caused by confluent monolayers of (530±25) Hz. The *insert* shows a fluorescent micrograph of a confluent MDCK-II cell monolayer stained for the tight junction associated protein ZO-1. The fluorescent probe clearly indicates cell boundaries, thus allowing one to determine the geometrical surface area of single cells. The scale *bar* represents 20 μm

about 600 Hz if $1.5 \cdot 10^6$ cells $\cdot$ cm^{-2} were seeded. For cell numbers larger than $4 \cdot 10^5$ cells $\cdot$ cm^{-2} the resonance frequency passes through a transient minimum, a phenomenon that becomes even more prominent for 3T3-cells (compare Fig. 6a). From these experiments we conclude that the shift in resonance frequency upon loading the resonator with a suspension of MDCK-cells is predominantly due to their specific or unspecific adhesion to the quartz surface, whereas the adsorption of medium ingredients to the

Table 1 Results of the adhesion isotherms for MDCK-I, MDCK-II and 3T3 cells as determined using the two case approach. $\Delta f_{monolayer}$ represents the maximum frequency shifts (as represented by the horizontal regression lines shown in the adhesion isotherms) arising from the attachment of the particular cell types for cell numbers sufficient to form a confluent monolayer. (Δf_{max} /ΔN) represents the slope of the ascending regression lines in the adhesion isotherms. The intersection of the horizontal and the ascending regression line for either cell type is given in the third column indicating the number of cells necessary to form a confluent monolayer as deduced from QCM-measurements. The fourth column represents the geometrical surface area of a single cell (±SDM) as determined from microscopic images and the corresponding number of cells per cm^2 in the last column

	$\Delta f_{monolayer}$ (Hz)	$\Delta f_{max}/\Delta N$ (Hz/cells $\cdot$ $cm^{-2} \cdot 10^{-3}$)	Intersection (cells $\cdot$ $cm^{-2} \cdot 10^5$)	Surface area (μm^2)	Cell number (cells $\cdot$ $cm^{-2} \cdot 10^5$)
MDCK-II	530±25	1.2±0.1	4.3±0.5	180±10 (n=79)	5.5±0.3
MDCK-I	320±20	1.0±0.1	3.1±0.4	270±15 (n=70)	3.7±0.2
3T3	240±15	1.3±0.3	1.9±0.5	745±30 (n=37)	1.3±0.1

evaporated gold electrode is of neglectable influence. Figure 3b shows the maximum frequency shift Δf_{max} dependent on the number of MDCK-II c ells seeded onto the quartz surface. The adhesion curve given in Fig. 3b exhibits saturation characteristics. For cell numbers up to $4 \cdot 10^5$ cells $\cdot$ cm^{-2} the change of the resonance frequency is approximately linearly dependent on the number of seeded cells, but approaches a final value between 500–600 Hz with further increasing cell numbers. Since the quartz resonator with the evaporated gold electrodes on both sides is almost opaque, it is impossible to document surface coverage by ordinary phase contrast microscopy. We therefore performed a correlation experiment on a transparent substrate. Figure 4 shows typical phase contrast micrographs of MDCK-II cells 5 hours after seeding cell suspensions with increasing cell numbers into chambered microscope slides of comparable geometric dimensions as the quartz dishes (A: $8.5 \cdot 10^4$ cells $\cdot$ cm^{-2}; B: $1.7 \cdot 10^5$ cells $\cdot$ cm^{-2}; C: $3.4 \cdot 10^5$ cells $\cdot$ cm^{-2}; D: $6.7 \cdot 10^5$ cells $\cdot$ cm^{-2}). As the surfaces of the microscope slides are not covered homogeneously with adherent cells, we had to select pictures that depict representative areas of the total growth area. Whereas the cell layers in micrographs A to C ($\leq 3.4 \cdot 10^5$ cells $\cdot$ cm^{-2}) are subconfluent with increasing surface coverages (A→C), micrograph D shows a confluent monolayer established after seeding $6.7 \cdot 10^5$ cells $\cdot$ cm^{-2} (non adherent cells were rinsed off before taking the picture). Comparing the given micrographs with the adhesion curve shown in Fig. 3b reveals that the QCM is obviously only sensitive to cells that are in close contact with the quartz surface, but does not detect cells that settle down on an already established cell layer. An excess of cells does not produce any further significant frequency shift as documented by the approximately horizontal part of the adhesion curve. Similar observations were reported by Rede-

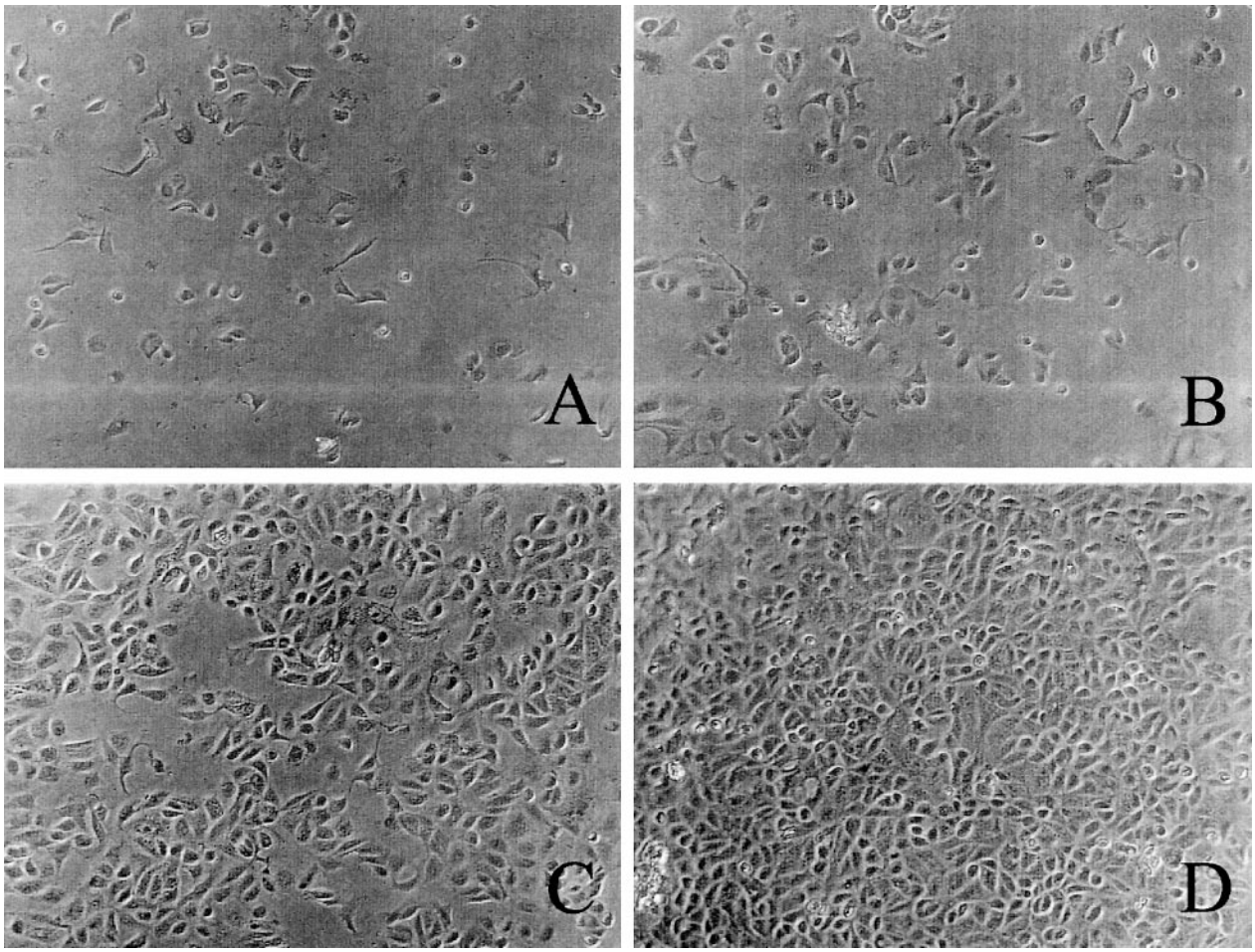

Fig. 4A–D Phase contrast micrographs of MDCK-II cells 300 minutes after seeding increasing cell numbers into chambered microscope slides. As the quartz dishes are almost opaque due to the evaporated gold electrodes on both sides of the crystal, we used this correlation experiment to demonstrate the situation at the surface for different seeding densities. Seeding densities in cells · cm^{-2}. A: $8.5 \cdot 10^4$; B: $1.7 \cdot 10^5$; C: $3.4 \cdot 10^5$; D: $6.7 \cdot 10^5$. Size of each picture is 553 μm×422 μm

penning et al. (1993) using rat osteoblasts. Our results confirm their conclusion that the shear wave does not propagate into the culture medium above the cell monolayer with a significant amplitude. We therefore analyzed the data shown in Fig. 3b by a simple two case approach, each of which is represented by a straight line. The straight line with the positive slope approximates the region of the curve in which the resonator surface is gradually covered by the seeded cells. The horizontal line, however, represents conditions under which the resonator surface is completely covered by a monolayer of MDCK-II cells and the surplus of cells, not contributing to the monolayer, does not affect the resonance frequency. Using this approach we computed for the slope of the regression line $(1.2 \pm 0.1) \cdot 10^{-3}$ Hz per cells · cm^{-2} and a maximum frequency shift of (530±25) Hz. The intersection of the two lines appears at $(4.3 \pm 0.5) \cdot 10^5$ cells · cm^{-2}, indicating the number of cells necessary to establish a confluent monolayer. From fluorescent micrographs of ZO-1 immunostained MDCK-II cells, as typically shown in the insert of Fig. 3b, we determined the average surface area of a single MDCK-II cell within a confluent monolayer to be (180 ± 10) μm^2 (mean ± SDM; $n = 79$) approximating the cell boundaries, as indicated by the fluorescent probe, to describe the cell perimeter at the substrate. From these data it is possible to calculate the number of cells per cm^2 in a confluent monolayer of MDCK-II cells to $(5.5 \pm 0.3) \cdot 10^5$ cells · cm^{-2} which reasonably fits to the QCM-results. The results of QCM measurements and geometric analysis are summarized in Table 1.

MDCK-I

Figures 5a and b depict the time courses of the resonance frequency and the resulting adhesion curve as recorded for MDCK-I cells in the same set of experiments as described in the previous section. The frequency shift upon adhesion of MDCK-I cells onto the resonator surface shows basically the same type of time course and adhesion curve as already discussed for MDCK-II cells. The slope of the ascending line amounts to $(1.0 \pm 0.1) \cdot 10^{-3}$ Hz per cell · cm^{-2} and is therefore not significantly different from the value

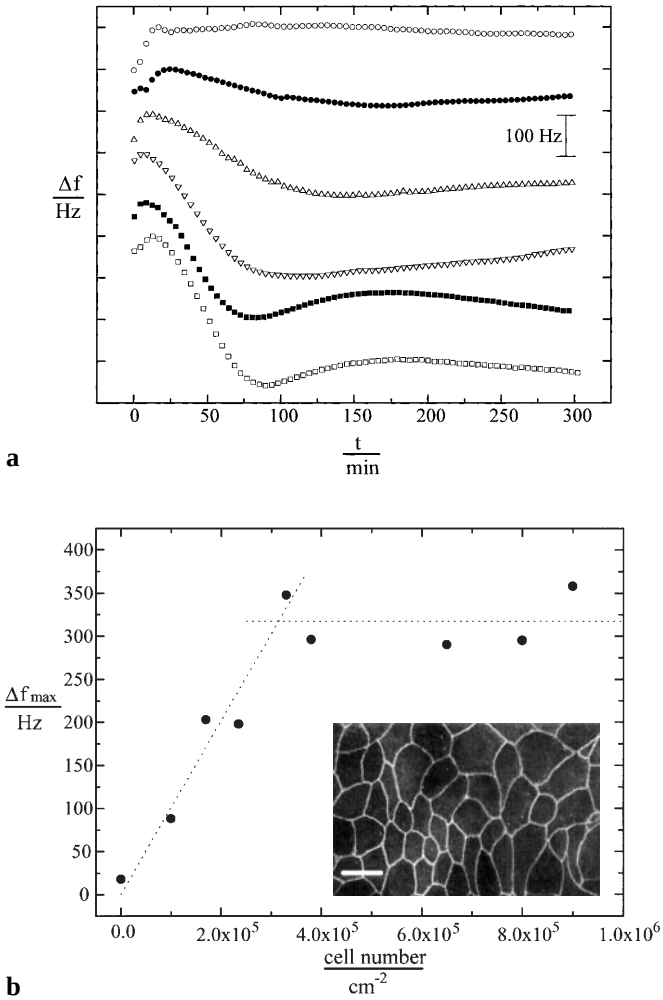

Fig. 5 **a** Time courses of the resonance frequency upon adhesion of increasing numbers of MDCK-I cells seeded into the quartz dish at time zero. The curve at the very top of the diagram (○), same as in Fig. 4a) depicts the time course of the resonance frequency without addition of cells for easy comparison. The corresponding seeding densities in cells per cm^2: $1.0 \cdot 10^5$ (●); $1.7 \cdot 10^5$ (△); $3.8 \cdot 10^5$ (▽); $6.3 \cdot 10^5$ (■); $9.0 \cdot 10^5$ (□). **b** Maximum frequency shift as deduced from the time courses shown in part **a** as a function of seeding density for MDCK-I cells. The *dotted lines* represent regression lines according to the two case approach. The slope of the ascending line amounts to $(1.0 \pm 0.1) \cdot 10^{-3}$ Hz/cells $\cdot$ cm^{-2}. The *horizontal line* depicts the maximum frequency shifts for confluent monolayers of (320 ± 20) Hz. The *insert* shows a fluorescent micrograph of MDCK-I cells stained for the tight junction associated protein ZO-1. The scale *bar* represents 20 μm

for MDCK-II cells. A significant deviation with respect to MDCK-II cells was observed for the maximum frequency shift for an entirely covered quartz resonator, as deduced from the horizontal line within the adhesion curve. Whereas a monolayer of MDCK-II cells induces a frequency shift of about (530 ± 25) Hz, MDCK-I cells decrease the resonance frequency only by (320 ± 20) Hz. The intersection of the two lines – indicating the number of cells in a confluent monolayer – appears at $(3.1 \pm 0.4) \cdot 10^5$ cells $\cdot$ cm^{-2}. Geometric analysis of MDCK-I monolayers reveals an average cell size of (270 ± 15) μm^2 (mean ± SDM; $n = 70$) which corresponds to a cell density of $(3.7 \pm 0.2) \cdot 10^5$ cells $\cdot$ cm^{-2}. Again a good correlation between the QCM experiments and geometric considerations is achieved. Results are summarized in Table 1.

Swiss 3T3-fibroblasts

Figure 6A and B depict the same set of curves as described above for MDCK-I and MDCK-II cells now for murine 3T3-fibroblasts upon adhesion onto the quartz surface. The adhesion curve reveals that the maximum frequency shift for this cell type is (240 ± 15) Hz which is even lower than the corresponding value for MDCK-I cells. The slope of the ascending line amounts to $(1.3 \pm 0.3) \cdot 10^{-3}$ Hz per cell $\cdot$ cm^{-2} and the intersection of the lines is at about $(1.9 \pm 0.5) \cdot 10^5$ cells $\cdot$ cm^{-2}. These findings are consistent with our microscopical studies of this cell type which revealed that the average surface area occupied by one 3T3-cell is about (745 ± 30) μm^2 (mean ± SDM; $n = 40$). The number of cells per cm^2 can therefore be estimated to be $(1.3 \pm 0.1) \cdot 10^5$ cells $\cdot$ cm^{-2}, in good agreement with the outcome of the QCM-experiment. Data are summarized in Table 1.

Cell adhesion in the presence of RGD-related peptides

In the second part of this study we addressed the question of whether or not the cells have to firmly attach onto the quartz surface by focal contacts to exert their influence on the shear oscillation of the quartz resonator or if the presence of the cellular body in close vicinity to the resonator surface is already sufficient to induce a shift in resonance frequency due to the altered microenvironment at the solid-liquid-interface. We therefore made use of an experimental assay recently described by Pierschbacher and Ruoslahti (1984), who studied the adhesion of NRK fibroblasts onto fibronectin coated surfaces and its inhibition by soluble peptide fragments of the fibronectin molecule. Within this and further studies (Ruoslahti and Pierschbacher 1987) the authors could demonstrate that the cell attachment activity of fibronectin is localized within the four amino acid sequence RGDS (Arg-Gly-Asp-Ser), in which the Ser-residue is not essential, but only conservative substitution is compatible with activity. This cell attachment peptide sequence was also shown to be present in other extracellular matrix proteins (e.g. laminin, vitronectin, collagens, thrombospondin etc.), so that it is nowadays regarded as a major motif in the molecular mechanisms of cell-substrate-adhesion. On the cellular side binding to extracellular matrix proteins is mediated by a whole family of transmembrane proteins, the so called integrins. These $\alpha\beta$-heterodimeric proteins connect the intracellular cytoskeleton to the extracellular matrix and therefore provide the mechanical stability of cell-substrate-adhesion (Hynes 1992). Among the integrins known so far there are several species that interact with the ECM-proteins via the RGDS-binding domain. Using our QCM-apparatus we investigated the time course of cell adhesion for MDCK-II cells in the presence

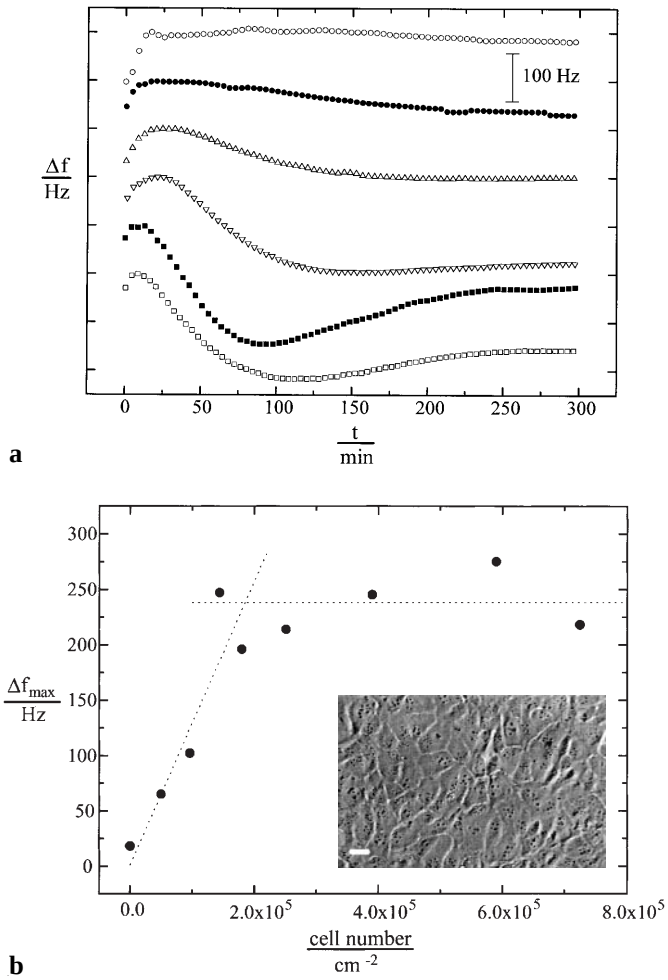

Fig. 6 **a** Time courses of the resonance frequency upon attachment of increasing numbers of 3T3-fibroblasts seeded into the quartz dish at time zero. Again the curve at the very top of the diagram (○), depicts the time course of the resonance frequency without addition of cells for comparison. Seeding densities in cells per cm^2: $5 \cdot 10^4$ (●); $1.0 \cdot 10^5$ (△); $1.8 \cdot 10^5$ (▽); $4.0 \cdot 10^5$ (■); $7.3 \cdot 10^5$ (□). Not all time courses considered in the following diagram **b** are depicted. **b** Maximum frequency shift as deduced from the time courses shown in part **a** as a function of seeding density for 3T3-cells. *Dotted lines* represent regression lines according to the two case approach as detailed in the text. The slope of the ascending line amounts to $(1.3 \pm 0.3) \cdot 10^{-3}$ Hz/cells $\cdot$ cm^{-2}. The *horizontal line* depicts the frequency shifts for confluent monolayers of (240±15) Hz. The *insert* shows a phase contrast micrograph of a confluent 3T3-cell monolayer as was typically used to determine the geometrical surface area of a single cell. The scale *bar* represents 20 μm

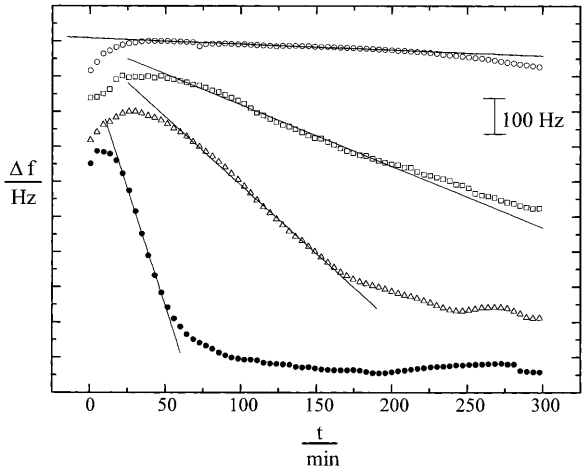

Fig. 7 Time courses of the resonance frequency upon seeding comparable numbers of MDCK-II cells (~$8 \cdot 10^5$ cells $\cdot$ cm^{-2}) into the quartz dishes at time zero. The particular cell suspensions were additionally supplemented with 1 mM of the pentapeptide Gly-Arg-Gly-Asp-Ser (GRGDS) (○), 1 mM (△) or 2 mM (□) of the tripeptide Arg-Gly-Asp (RGD), or 1 mM of the pentapeptide Ser-Asp-Gly-Arg-Gly (SDGRG) (●). The *solid lines* represent the linear regressions to estimate the rate of cell attachment

Table 2 Rate of the frequency decrease upon attachment of MDCK-II cells to the quartz crystal in the presence of 1 mM Ser-Asp-Gly-Arg-Gly (SDGRG), 1 mM Arg-Gly-Asp (RGD), 2 mM Arg-Gly-Asp and 1 mM Gly-Arg-Gly-Asp-Ser (GRGDS) as deduced from the shifts of the resonance frequency shown in Fig. 7

Peptide	$\Delta f(t)/\Delta t$ (Hz/min)
1 mM SDGRG	–13.0
1 mM RGD	–3.9
2 mM RGD	–1.7
1 mM GRGDS	–0.2

of three different RGD-related peptides. Figure 7 depicts typical time courses of the resonance frequency shift upon seeding comparable cell numbers (~$8 \cdot 10^5$ cells $\cdot$ cm^{-2}) into the resonator dishes at time zero. The particular cell suspensions were supplemented with 1 mM (△) or 2 mM (□) of the tripeptide RGD, 1 mM of the pentapeptide GRGDS (Gly-Arg-Gly-Asp-Ser) (○) or 1 mM of the pentapeptide SDGRG (Ser-Asp-Gly-Arg-Gly) (●), which contains the same amino acid residues as GRGDS but in the reverse order. Comparing the shift in resonance frequency for 1 mM SDGRG with the curve for a similar cell number but in the absence of any additional peptide in Fig. 3a reveals that the presence of this peptide does not significantly alter the time course of the frequency shift, indicating that the adhesion of MDCK-II cells remains unaffected. However, 1 mM of the pentapeptide GRGDS almost completely inhibits cell adhesion to the resonator surface within the observation time. Competitive inhibition of the integrin binding domain by the soluble GRGDS-pentapeptide obviously abolishes the ability of MDCK-II cells to firmly attach to the surface and to cause a significant shift of the resonance frequency. In a correlation experiment using microscopic inspection of a transparent substrate, we could verify that under these conditions the cells do not attach to the surface. Figure 7 furthermore shows that addition of 1 and 2 mM of the tripeptide RGD gradually interferes with the time course of the frequency shift and therefore with the cell adhesion process. However, even 2 mM concentrations of the tripeptide can not completely inhibit cell attachment but cause a considerable delay. In order to describe the influence of the three different peptides more quantitatively, we determined the slope of the linear parts of the time courses shown in Fig. 7 to get a measure for the rate of cell adhesion to the substrate (Table 2). For the

adhesion experiment in the presence of 1 mM SDGRG the slope of the regression line amounts to (–13.0) Hz/min, whereas in the presence of 1 mM GRGDS it is reduced to (–0.2) Hz/min. The corresponding values for the experiments in the presence of 1 mM and 2 mM RGD were (–3.9) Hz/min and (–1.7) Hz/min, respectively.

Discussion

General considerations

The present study is intended to investigate the applicability of the quartz crystal microbalance in the active oscillator mode to monitor and quantify the attachment and spreading of anchorage dependent cells to a solid substrate in real time. As model systems we chose three very popular cell lines derived from epithelial (MDCK) or connective tissue (Swiss-3T3). For any of the three different cell species we could follow their attachment to the quartz surface by the time course of the resonance frequency (Figs. 3a, 5a, 6a). Each of these curves is characterized by an initial increase of the resonance frequency due to thermal equilibration of the cell suspension to 37 °C after mounting the quartz dish into the temperature controlled Faraday cage. We are well aware of the fact that this initial increase of the resonance frequency may mask the very first features of cell adhesion and is therefore responsible for some inaccuracy of the measurement close to time zero. Trying to overcome these problems we considered the approach recently described by Redepenning et al. (1993), who allowed the quartz resonator to stabilize in contact with air at ambient temperature and added the cell suspension subsequently. The resulting shift of the resonance frequency was then followed with time also at ambient temperature and was therefore unaffected by thermal effects. We also investigated the time course of cell adhesion for MDCK-II cells at 27 °C and the resulting curve is shown in Fig. 8 in comparison with an experiment performed at 37 °C. The initial increase of the resonance frequency is no longer present in the experiment at 27 °C (Fig. 8: ○) but the reduced temperature also considerably affects the time course of subsequent cell attachment. Owing to the minor physiological relevance of cell adhesion studies at temperatures significantly different from 37 °C, this approach was not attractive for us. Gryte et al. (1993) also performed adhesion studies at 37 °C using African Green Monkey kidney (Vero) cells. These authors filled the quartz dish with an aliquot of the cell culture medium and after resonance frequency and temperature had stabilized, the cell suspension was added accompanied by perturbations of the resonance frequency taking about ten minutes to regain equilibrium. In our hands a procedure like this leads to additional frequency fluctuations that we did not observe using our approach. Adding a cell suspension to an already equilibrated quartz crystal is only possible if the quartz dish is loosely closed, as any further handling produces severe perturbations of the resonance frequency. A loose

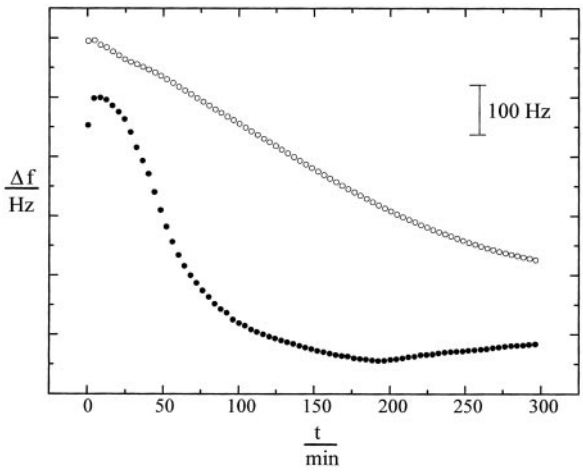

Fig. 8 Time course of the resonance frequency upon attachment of $4.5 \cdot 10^5$ MDCK-II cells per cm^2 onto the resonator surface at 27 °C (○). The initial increase of the resonance frequency as shown in the preceeding curves is absent when performing the experiment close to room temperature. However, obviously the rate of cell attachment is also significantly influenced due to the lower temperature as indicated by the diminished rate of the frequency shift. For comparison, the *filled circles* (●) represent the shift of the resonance frequency upon attachment of $3.7 \cdot 10^5$ cells $\cdot$ cm^{-2} of MDCK-II cells when the experiment is performed at 37 °C

coverage may allow slight evaporation of the culture medium, especially at 37 °C. Since it has recently been shown (Lin and Ward 1995; Schneider and Martin 1995) that alterations in fluid height in the submicrometer range may cause periodic frequency fluctuations as well as long-term drifts, a tight closure of the measuring chamber seems to be necessary.

We addressed the question of whether the adhesion of the cells to the surface itself or their sedimentation from the bulk phase to the electrode is the rate determining step within our experimental system. To get an estimate we regarded the cell suspension as a homogeneous, monodisperse suspension of spherical particles with radius r_c and density ρ_c and used the Stokes equation to calculate their rate of sedimentation v_c:

$$v_c = \frac{2}{9}\, g\, \frac{(\rho_c - \rho_m)\, r_c^2}{\eta_m} \qquad (3)$$

Herein g accounts for the acceleration due to gravity, ρ_c is the density of the cells, ρ_m and η_m are the density and viscosity of the culture medium, respectively, r_c is the hydrodynamic radius for the particular cell type. Densities and hydrodynamic radii for the individual cell types are summarized in Table 3. For η_m and ρ_m we used the corresponding values of water at 37 °C [$\rho = 0.993$ g/cm^3; $\eta = 0.692$ mPa $\cdot$ s)] (Weast 1984). Equation (3) provides sedimentation rates of $4.0 \cdot 10^{-2}$ cm $\cdot$ min^{-1} for MDCK-II, $5.3 \cdot 10^{-2}$ cm $\cdot$ min^{-1} for MDCK-I and $7.8 \cdot 10^{-2}$ cm $\cdot$ min^{-1} for 3T3 fibroblasts, reflecting the increasing hydrodynamic radii for the particular cell types (Table 3). Times t_{max} necessary for a cell to descend from the very top of the quartz dish to the surface of the electrode ($h = 1.5$ cm)

Table 3 Densities ρ_c and hydrodynamic radii r_c (±SDM) for MDCK-I, MDCK-II and 3T3 cells as used to estimate cellular sedimentation behavior using Eq. (3). t_{max} represents times necessary for either cell species to descend from the very top of the quartz dish to the resonator surface ($h = 1.5$ cm). Due to the not entirely cylindrical geometry of the quartz dishes used in the present study and detailed in the text, we also calculated sedimentation times $t_{75\%}$ necessary for about 75% of the seeded cells to reach the resonator surface. η_{app} represents the apparent viscosity of the different cell layers as determined from the frequency shifts for confluent monolayers using the Gordon-Kanazawa equation (2) together with the calibration curve shown in Fig. 2

	ρ_c (g/cm^3)	r_c (μm)	t_{max} (min)	$t_{75\%}$ (min)	η_{app} (mPa · s)
MDCK-II	1.051±0.005	5.8±0.1 (n=45)	38±4	23±2	1.86±0.08
MDCK-I	1.053±0.005	7.0±0.3 (n=62)	28±4	17±2	1.29±0.05
3T3	1.050±0.005	8.6±0.2 (n=59)	19±2	12±1	1.12±0.04

range between 38 min for MDCK-II and 19 min for 3T3. These values, however, need some additional considerations: (i) As our quartz dishes are not entirely cylindrical (the upper part of the dish is of reduced diameter) only a diminished portion of cells has to descend from the very top of the dish. Approximately 75% of the cells are within 0.9 cm of the quartz surface. We therefore additionally calculated the times ($t_{75\%}$) which are necessary for 75% of the seeded cells to reach the surface of the quartz resonator. (ii) In cases when we seeded more cells than necessary to form a confluent monolayer (see Table 1) only those cells arriving at the surface at early times will find a free attachment site. Therefore only a corresponding fraction of the sedimentation time is necessary to achieve a sufficiently high number of cells at the surface to form a cell monolayer. For example, we considered the case when $1.5 \cdot 10^6$ cells · cm^{-2} of MDCK-II are seeded into the quartz dish at time zero (Fig. 3a, □). Using the approximations mentioned above, it takes not more than 10 min for the first $5 \cdot 10^5$ cells · cm^{-2} – sufficient to form a complete monolayer – to reach the resonator surface, whereas the maximum frequency shift is not achieved before 60 minutes after plating. We conclude that even for MDCK-II cells with the smallest sedimentation rate, the time course of the resonance frequency mainly reflects the time course of cell attachment to the resonator surface.

Another interesting feature within the time courses of the resonance frequencies is the appearance of a transient minimum for larger seeding densities. Comparable observations were reported by Giaever and Keese (1986) and Pei et al. (1994) who investigated the time course of cell attachment for WI-38 and NIH-3T3-fibroblasts using the ECIS method as described in the introduction. Following the opinion of these authors, the cells first attach to the surface rather firmly but then loosen their substrate contact. A similar process might be responsible for the appearance of a minimum in the time course of the resonance frequency. These rearrangements obviously do not occur when seeding densities are too low to establish a confluent monolayer. Therefore we chose to analyze the maximum frequency change for a particular cell density rather than its value at the end of the experiment to make data for confluent and subconfluent monolayers more comparable. These observations additionally indicate that the QCM-technique is not only sensitive to the number of adherent cells but also reflects changes of cell-substrate interactions.

Adhesion curves

We analyzed the adhesion curves derived from the time courses of the resonance frequency and shown in Figs. 3b, 5b and 6b by means of two straight lines, one representing the situation for seeding densities not sufficient to establish a confluent monolayer and the second – horizontal one – describing the situation for an excess of cells. We chose this simple analytical approach as it is rather complex to model the attachment of cells from suspension to a solid substrate for different seeding densities and requires extensive and very detailed microscopic investigations for either cell type. The two-line-approximation seems to be appropriate and is confirmed by the good agreement to the geometrical considerations derived from micrographs of confluent cell monolayers. Deviations from the regression lines may be due to the fact that the cell suspensions were not ideally homogeneous and monodisperse, as cell clustering is not completely avoidable. This becomes even more important as it is well known that the piezoelectrically active surface is not evenly sensitive over its entire area. The differential mass sensitivity peaks at the centre of the electrode and declines towards its edges which was empirically described by a Gaussian distribution (Martin and Hager 1988). Slightly different surface roughnesses of the quartz resonators used in the various experiments might also account for some deviations.

As detailed in Table 1 the frequency shift achieved for confluent cell monolayers is dependent on the particular cell type ranging between 240 Hz for 3T3-cells to 530 Hz for MDCK-II cells. Comparison of available literature data for different cell types is complicated by the fact that different oscillator circuits (supporting different resonance frequencies), different experimental setups and also different external conditions were used and any of these can markedly influence the outcome of the experiment. As all experiments presented in this study were performed under exactly the same conditions, the observed differences can unequivocally be attributed to individual characteristics of the different cell species. Thus, the question arises of what are the factors that are responsible for the individual QCM signals. There are some basic electromechanical models available that allow one to relate the experimentally observed frequency shift to quantities characterizing the surface attached material. Recently, we could experimentally prove by impedance analysis (Janshoff et al. 1996) that cell monolayers attached to quartz resonators do not behave like a rigid mass loading and that the Sauerbrey equation (1) is therefore not applicable, as has been argued by oth-

ers. The presence of a cell layer on top of a quartz resonator was shown to cause a distinct damping of the shear displacement as is well known for viscous fluids. We therefore described the attached cell layer like a continuous viscous material and could calculate its apparent viscosity from impedance data of the cell covered resonator and equivalent circuit modelling. However, a more detailed analysis revealed some deviations between the cellular system and the assumed model. Despite these findings we here apply the Gordon-Kanazawa equation (2) – derived for viscous fluids in contact to the resonator – to calculate the density-viscosity products of the different cell layers using the calibration with glycerol/water mixtures (Fig. 2). Since the frequency shifts associated with the established cell layers are relative to an immersion of the resonator in pure culture medium, the density-viscosity-products of the cell layers, as calculated from Eq. (2), need correction for the corresponding quantity of the culture medium, which we approximate by the values of pure water $\{(\eta \cdot \rho)_{water} = 6.9 \cdot 10^{-4}$ (Pa · s · g/cm^3)$\}$. Using the densities of the particular cell types (Table 3), it is possible to compute their apparent viscosities ranging between 1.9 mPa · s for MDCK-II to 1.1 mPa · s for 3T3 cells (Table 3). These values agree with those given by Redepenning et al. (1993) for rat osteoblasts ($\eta_{app} = 3$ mPa · s) at ambient temperature, also applying the Gordon-Kanazawa equation to their QCM data. The apparent viscosities from QCM-measurements are in the same range as cytoplasmic viscosities determined from rotational or translational mobility of fluorescent probes ($\eta_{app} = 1-9$ mPa · s) (Periasamy et al., 1992), but are orders of magnitude smaller compared to values that were determined for granulocytes using micropipette aspiration ($\eta_{app} = 2 \cdot 10^5$ mPa · s) (Evans and Yeung 1989). Modelling adherent mammalian cells as a purely viscous loading of the resonator assumes direct and continuous contact between the ventral side of the cell and the resonator surface. It is, however, well known that there is a considerable gap between plasma membrane and culture substrate providing an aqueous/proteinaceous intermediate layer that is not considered in the simple model. As we do not know thus far about the decay length of the shear wave in such a composite system, we can not account for the individual contributions of the different subcellular compartments. Thus, we think that a complete description of cell monolayers on top of quartz resonators requires a two or three layer model to distinguish between mechanical properties of the cellular body and those of the underlying layer. It is reasonable to assume that the thickness and the mechanical properties of the layer between cell and substrate in concert with the individual adhesion characteristics will be of decisive importance for the QCM response of adherent cells but are not accessible so far.

Cell adhesion in the presence of competitive inhibitory peptides

Studying cell attachment to the resonator surface in the presence of RGD-related peptides (see Fig. 7) revealed that only firm attachment of the cells to the quartz crystal causes a shift of the resonance frequency whereas competitive inhibition of integrin binding sites by 1 mM GRGDS abolishes a change of the resonance frequency. From the undisturbed adhesion of MDCK-II cells in the presence of 1 mM SDGRG we conclude that this effect is highly specific and not due to differences in unspecific electrostatic interactions between the cell surface and the substrate, as the two peptides only differ in the order of the same amino acid residues bearing identical charge densities. As we did not precoat the resonator surface with any ECM-protein, the very rapid deposition of proteins from the culture medium (supplemented with serum) (Taylor 1961) to the resonator surface provides the binding sites for cellular attachment. For instance, it is well known that vitronectin, a major plasma glycoprotein that contains the RGDS recognition sequence, adsorbs strongly from solution to glass and other surfaces used in tissue culture (Tomasini and Mosher 1991).

Comparing the time courses of the frequency shifts for 1 mM GRGDS on the one hand and 1 and 2 mM RGD on the other hand, it is obvious that GRGDS is a more potent inhibitor of cellular attachment. As it is reasonable to assume for comparable experimental conditions that the binding constant of the ligand-receptor-couple is lower for the RGD tripeptide than for the GRGDS pentapeptide, the stronger influence of GRGDS is reasonable and compatible with literature data (Pierschbacher and Ruoslahti 1984). Thus, the inhibitory effects of the RGD and GRGDS-peptides on cell attachment can easily be monitored and quantified by analysis of cell attachment kinetics as accessible using a quartz crystal microbalance.

Conclusion

The present study demonstrates that the QCM-technique in the active oscillator mode is a simple and very versatile in situ method to monitor and quantify the attachment and spreading of adherent cells to a solid substrate with high time resolution. In the future it may become a very useful tool to study the adhesion behavior of cells to quartz resonators with different surface composition as the gold electrodes provide a multitude of possibilities to immobilize different compounds (e.g. ECM-proteins, polymers etc.). Development of devices capable of recording the frequency response of more than one quartz resonator within an experimental run may provide a powerful screening system to test for compounds that interfere with cell adhesion. However, there is strong need for further studies directed towards a more detailed understanding on the cellular characteristics that are responsible for their particular QCM-signals.

Acknowledgements This work has been financially supported by the Deutsche Forschungsgemeinschaft (SFB 293). J. W. is recipient of a grant provided by the Studienstiftung des Deutschen Volkes, A. J. was supported by a scholarship granted by the Fonds der Chemischen Industrie. The authors are very much indebted to Dipl.-Ing.

W. Willenbrinck, Dipl.-Ing. W. Wilting, Dr. F. Höhn and Dr. M. Sieber for their expert help with all kinds of electronic problems and for helpful discussions.

References

Aplin JD, Campbell S, Foden LJ (1984) Adhesion of amnion epithelial cells to extracellular matrix. Exp Cell Res 153: 425–438

Buttry DA, Ward MD (1992) Measurement of interfacial processes at electrode surfaces with the electrochemical quartz crystal microbalance. Chem Rev 92: 1355–1379

Cornell R (1969) Cell-substrate adhesion during cell culture. Exp Cell Res 58: 289–295

Deakin MR, Buttry DA (1989) Electrochemical applications of the quartz crystal microbalance. Anal Chem 61/20: 1147A–1154A

Evans E, Yeung A (1989) Apparent viscosities and cortical tension of blood granulocytes determined by micropipet aspiration. Biophys J 56: 151–160

Gallez D (1994) Non-linear stability analysis for animal cell adhesion to solid support. Colloids and Surfaces B: Biointerfaces 2: 273–280

Giaever I, Keese Cr (1986) Use of electric fields to monitor the dynamical aspect of cell behavior in tissue culture. IEEE Trans Biomed Eng 33: 242–247

Gryte DM, Ward MD, Hu WS (1993) Real-time measurement of anchorage dependent cell adhesion using a quartz crystal microbalance. Biotechnol Prog 9: 105–108

Hillier AC, Ward MD (1992) Scanning electrochemical mass sensitivity mapping of the quartz crystal microbalance in liquid media. Anal Chem 64: 2539–2554

Hynes RO (1992) Integrins: versatility, modulation, and signaling in cell adhesion. Cell 69: 11–25

Janshoff A, Wegener J, Sieber M, Galla HJ (1996) Double mode impedance analysis of epithelial cell monolayers cultured on shear wave resonators. Eur Biophys J 25: 93–103

Kanazawa KK, Gordon JG (1985) Frequency of a quartz crystal microbalance in contact with liquid. Anal Chem 57: 1770–1771

Lin Z, Ward MD (1995) The role of longitudinal waves in quartz crystal microbalance applications in liquids. Anal Chem 67: 685–693

Martin BE, Hager HE (1988) Velocity profile on quartz crystals oscillating in liquids. J Appl Phys 65: 2630–2635

Matsuda T, Kishida A, Ebato H, Okahata Y (1992) Novel instrumentation monitoring in situ platelet adhesivity with a quartz crystal microbalance. ASAIO J 38: M171–M173

Mitra P, Keese CR, Giaever I (1991) Electric measurements can be used to monitor the attachment and spreading of cells in tissue culture. BioTechniques 11: 504–510

Muratsugu M, Romaschin AD, Thompson M (1997) Adhesion of human platelets to collagen detected by ^{51}Cr labelling and acoustic wave sensor. Anal Chim Acta 342: 23–29

Periasamy N, Pin Khao H, Fushimi K, Verkman AS (1992) Organic osmolytes increase cytoplasmic viscosity in kidney cells. Am J Physiol 263: C901–C907

Pei Z, Keese CR, Giaever I, Kurzawa H, Wilson DE (1994) Effect of the SV2-neo plasmid on NIH 3T3 cell motion detected electrically. Exp Cell Res 212: 225–229

Pierschbacher MD, Rouslahti E (1984) Cell attachment activity of fibronectin can be duplicated by small synthetic fragments of the molecule. Nature 309: 30–33

Poste G, Fidler IJ (1980) The pathogenesis of cancer metastasis. Nature 283: 139–146

Redepenning J, Schlesinger TK, Mechalke EJ, Puleo DA, Bizios R (1993) Osteoblast attachment monitored with a quartz crystal microbalance. Anal Chem 65: 3378–3381

Rouslahti E, Pierschbacher MD (1987) New perspectives in cell adhesion: RGD and integrins. Science 238: 491–497

Ruoslahti E, Hayman EG, Pierschbacher M, Engvall E (1982) Fibronectin: purification, immunochemical properties and biological activities. Methods Enzymol 82: 803–831

Sauerbrey G (1959) Verwendung von Schwingquarzen zur Wägung dünner Schichten und zur Mikrowägung. Z Phys 55: 206–222

Schneider TW, Martin SJ (1995) Influence of compressional wave generation on thickness-shear mode resonator response in a fluid. Anal Chem 67: 3324–3335

Taylor AC (1961) Attachment and spreading of cells in culture. Exp Cell Res Suppl 8: 154–173

Teuscher JH, Garell RL (1995) Stabilization of quartz crystal oscillators by a conductive adhesive. Anal Chem 67: 3372–3375

Tomasini BR, Mosher DF (1991) Vitronectin. Prog Hemost Thromb 10: 269–305

Vogler EA (1988) Thermodynamics of short-term cell adhesion in vitro. Biophys J 53: 759–769

Weast RC (1984) Handbook of chemistry and physics. CRC Press, Boca Raton (F1)

Wegener J, Sieber M, Galla HJ (1996) Impedance analysis of epithelial and endothelial cell monolayers cultured on gold surfaces. J Biochem Biophys Methods 32: 151–170

Xu H, Schlenoff JB (1995) Kinetics, isotherms, and competition in polymer adsorption sing the quartz crystal microbalance. Langmuir 10: 241–245